scientific reports

Check for updates

OPEN

HIF1α activation in dendritic cells under sterile conditions promotes an anti-inflammatory phenotype through accumulation of intracellular lipids

Elizabeth G. Wood[1], Claire E. Macdougall[1], Hazel Blythe[1], Marc Clément[2], Romain A. Colas[1], Jesmond Dalli[1], Federica Marelli-Berg[1] & M. Paula Longhi[1]✉

Obesity is among the leading causes of elevated cardiovascular disease mortality and morbidity. Adipose tissue dysfunction, insulin resistance and inflammation are recognized as important risk factors for the development of cardiovascular disorders in obesity. Hypoxia appears to be a key factor in adipose tissue dysfunction affecting not only adipocytes but also immune cell function. Here we examined the effect of hypoxia-induced transcription factor HIF1α activation on classical dendritic cell (cDCs) function during obesity. We found that deletion of *Hif1α* on cDCs results in enhanced adipose-tissue inflammation and atherosclerotic plaque formation in a mouse model of obesity. This effect is mediated by HIF1α-mediated increased lipid synthesis, accumulation of lipid droplets and alter synthesis of lipid mediators. Our findings demonstrate that HIF1α activation in cDCs is necessary to control vessel wall inflammation.

Classical dendritic cells (cDCs) are the main antigen presenting cells and key regulators of immune homeostasis and immunity[1]. Constantly probing their surroundings, cDCs are poised to detect invading pathogens, initiate and direct adaptive immune responses. cDCs are found in peripheral tissue in an immature state, where they sense and sample the environment for self- and non-self-antigens. Under pathogen driven danger signals, e.g. toll-like receptor (TLR), cDCs undergo an intricate maturation process characterized by increased expression of co-stimulatory molecules, cytokine/chemokine production and enhanced migration to draining lymph nodes (dLN) to present antigen to naïve T cells[1]. In tissue, cDCs must adapt to specific metabolic cues such as nutrient restriction or low O_2 tensions, which may modulate their biological functions. Indeed, in recent years it became apparent that disruption of key metabolic pathways can alter immune cell activation and differentiation.

Reduced oxygen or hypoxia, is a hallmark of multiple acute and chronic diseases and arises especially in inflamed tissues. Cellular adaptation to hypoxia rely on stabilization of the hypoxia-inducible factor-1 (HIF1) transcription factor, which drives the metabolic changes required for adaptation to hostile microenvironments. HIF1 is a heterodimer transcription factor consisting of a constitutively expressed β-subunit (HIF1β) and an oxygen-regulated α subunit (HIF1α)[2]. Under normoxic conditions, HIF1α is regulated through hydroxylation of proline residues, ubiquitination and rapid degradation by the proteasome. Under low oxygen concentrations, however, prolyl hydroxylase is inactivated and HIF1α can translocate into the nucleus for transcriptional regulation. HIF1α accumulation does not always occur under low O_2 tension but can be triggered by oxygen-independent signalling events or cellular stress, such as toll-like receptor signalling and reactive oxidase species (ROS)—a phenomenon known as 'pseudohypoxia'[3].

Activation of the hypoxia pathway is believed to fuel inflammation, largely due to HIF1α activation in macrophages. Lipopolysaccharide (LPS) activation induces HIF1α protein accumulation in macrophages under normoxic conditions[4] leading to metabolic reprogramming, succinate release, and IL-1β production[5]. HIF1α-deficient macrophages exhibit impaired inflammatory responses, with reduced glycolytic rate, motility and migration[6]. Similarly, toll-like receptor (TLR) activation in dendritic cells, leads to HIF1α stabilization, glucose

[1]William Harvey Research Institute, Barts and the London School of Medicine and Dentistry, Queen Mary University of London, London EC1M 6BQ, UK. [2]INSERM U1148, Laboratory for Vascular Translational Science, Hôpital Bichat, 46 rue Henri Huchard, 75018 Paris Cedex, France. ✉email: m.longhi@qmul.ac.uk

uptake and glycolytic metabolic shift[7,8]. In this context, deletion of HIF1α results in decreased ATP production, cell survival and T cell priming[8–10]. However, the effect of HIF1α on dendritic cells function remains controversial. In other studies, particularly under hypoxic conditions, HIF1α activation has been shown to promote anti-inflammatory response[11,12]. HIF1α has pleiotropic effects regulating hundreds of genes encoding glycolytic enzymes, glucose transporters, matrix metalloproteinases, angiogenic and survival factors, that may depend on time and context. In addition, these divergent reports may in fact be explained by differences in experimental conditions or cell type targeted.

The present study was designed to investigate the role of HIF1α activation in cDCs in an experimental model of obesity by using mice with HIF1α deletion specifically in cDCs. Contrary to what was expected, deletion of HIF1α in cDCs promoted adipose tissue inflammation and atherosclerotic plaque formation. This effect was mediated by intracellular lipid accumulation and altered production of lipid mediators, which translated into reduced T cell stimulation.

Results

Deletion of *Hif1α* in cDCs leads to increased adipose tissue inflammation under high lipid and cholesterol diet. Adipose tissue hypoxia has been causally implicated in obesity-induced inflammation and insulin resistance. Under lipid rich diet, adipocyte expansion decreases oxygen tension and ROS production, which leads to rapid activation of HIF1α[13,14]. cDCs are present in visceral adipose tissue (VAT) where they control tissue homeostasis[15]. To investigate the effect of HIF1α in cDCs under chronic, sterile inflammation, we generated cDC-specific *Hif1α* knockdown by crossing *Zbtb46*-CRE with *Hif1α*$^{fl/fl}$ mice. As Zbtb46 is expressed in some non-haematopoietic cells, we performed mice chimeras where irradiated C57BL/6 mice were reconstituted with bone marrow cells from *Hif1α*$^{fl/fl}$ × Zbtb46-CRE (referred to as *Hif1α*$^{-/-}$) or *HIF1α*$^{fl/+}$ × Zbtb46-CRE (referred to as WT) mice. HIF1α deletion is shown in Suppl Fig. S1A. *Hif1α*$^{-/-}$ or WT mice were fed a lipid-rich diet (western diet) for 12 weeks, which resulted in HIF1α increase in cDCs (Fig. 1a). Surprisingly, deletion of HIF1α in cDCs results in increased immune cell infiltration into visceral adipose tissue (VAT) from *Hif1α*$^{-/-}$ mice, with increased numbers of cDCs, T cells and decreased regulatory T cells (Tregs) (Fig. 1b,c; Suppl Fig. S1b). Expression of the co-stimulatory molecule CD86 remained unchanged (Suppl Fig. S1c). Production of IL-17 in VAT-infiltrated T cells was increased in *Hif1α*$^{-/-}$ compared to WT mice together with increased IFNγ production in lymph nodes (LN) (Fig. 1d; Suppl Fig. S1d). No differences were observed in splenic T cells (Fig. 1d). This contributes to the enhanced VAT inflammation in *Hif1α*$^{-/-}$ mice as detected by RT-PCR (Fig. 1e).

Chronic inflammation in VAT plays a central role in the development of obesity-related insulin resistance and systemic metabolic abnormalities[16]. Thus, we evaluated if the increased inflammation in *Hif1α*$^{-/-}$ mice could translate into systemic metabolic abnormalities. Body and VAT weight were similar between mice (Suppl Fig. S1e,f). *Hif1α*$^{-/-}$ mice displayed a small increase in fasting glucose levels and serum insulin levels compared to WT mice, albeit this was not significant (Fig. 1g,h). Circulating concentrations of adiponectin were reduced in *Hif1α*$^{-/-}$ mice indicative of adipocyte dysfunction (Fig. 1f–h). Despite signs of metabolic misbalance, *Hif1α*$^{-/-}$ mice showed no sign of increased glucose and insulin tolerance during a glucose tolerance (GTT) and insulin tolerance (ITT) test (Suppl Fig. S1g,h). Thus, the results presented here indicate that inhibition of the Hif1 pathways under chronic, low oxygen conditions, promotes cDC activation.

Deletion of *Hif1α* in cDCs accelerates the development of atherosclerosis. Obesity-induced chronic inflammation is tightly linked to the development of atherosclerotic plaque[17]. The atherosclerotic plaque is characterized by arterial wall thickening, ROS production and reduced oxygen supply in certain areas of the vascular intima creating a hypoxic milieu[18]. HIF1α expression was observed in macrophages and smooth muscle cells bordering the necrotic core, and was associated with inflammation and angiogenesis[19]. In addition, arteries are surrounded by perivascular adipose tissue which, under metabolic abnormalities, appears to promote vascular dysfunction and atherosclerosis[20]. Thus, we hypothesized that increased VAT inflammation in *Hif1α*$^{-/-}$ mice might have a negative impact on the development of atherosclerosis. To test this, lethally-irradiated low density lipoprotein receptor knockout (*Ldlr*$^{-/-}$) mice were reconstituted with bone marrow from *Hif1α*$^{fl/fl}$ × Zbtb46-CRE (referred as *Hif1α*$^{-/-}$ → *Ldlr*$^{-/-}$) or HIF1α$^{fl/+}$ × Zbtb46-CRE mice (referred as WT → *Ldlr*$^{-/-}$). *Ldlr*$^{-/-}$ mice, under fat rich diet, are known to show elevated plasma cholesterol (25 mmol/L) and rapid atherosclerotic plaque formation[21].

Hif1α$^{-/-}$ → *Ldlr*$^{-/-}$ and WT → *Ldlr*$^{-/-}$ were fed a WD for 12 weeks, after which the presence of hypoxic cDCs in the atherosclerotic lesions was confirmed by pimonidazole staining (Fig. 2a). In agreement with increased VAT inflammation *Hif1α*$^{-/-}$ → *Ldlr*$^{-/-}$ mice had greater numbers of cDCs and T cells in atherosclerotic lesions compared to WT → *Ldlr*$^{-/-}$ mice (Fig. 2b). The ratio of cDC subsets remains unchanged between *Hif1α*$^{-/-}$ → *Ldlr*$^{-/-}$ and control mice as well as the expression of CD86 (Suppl Fig. S2a,b). This was accompanied by enlarged draining lymph nodes (dLN) and increased T cell-mediated IFNγ production in *Hif1α*$^{-/-}$ → *Ldlr*$^{-/-}$ mice compared to controls (Fig. 2c; Suppl Fig. S2c). No differences were observed in the spleen (Fig. 2c; Suppl Fig. S2c). The numbers of LN migratory DCs (mDCs) and their CD86 expression remained constant (Suppl Fig. S2d,e). However, intracellular levels of IL12 were elevated in VAT-cDCs and mDC in *Hif1α*$^{-/-}$ → *Ldlr*$^{-/-}$ compared to control mice (Suppl Fig. S2f). Accordingly, *Hif1α* deficiency in cDCs was associated with a significant increase in atherosclerotic lesion development compared to control (Fig. 2d–f). Plasma cholesterol levels were comparable between the groups of mice (Fig. 2g). Similar to abdominal VAT, inflammatory markers in perivascular fat were increased in *Hif1α*$^{-/-}$ → *Ldlr*$^{-/-}$ compared to WT → *Ldlr*$^{-/-}$ mice (Fig. 2h).

To confirm that this phenotype was a consequence of increased cDC activation, we tested cDC T cell stimulatory capacity in vivo. Enhanced proliferation of ovalbumin (OVA)-specific CD4^{+} T cells (OT-II) could be observed in the aorta, VAT and dLN but not spleen from *Hif1α*$^{-/-}$ → *Ldlr*$^{-/-}$ compared to control mice (Fig. 2i).

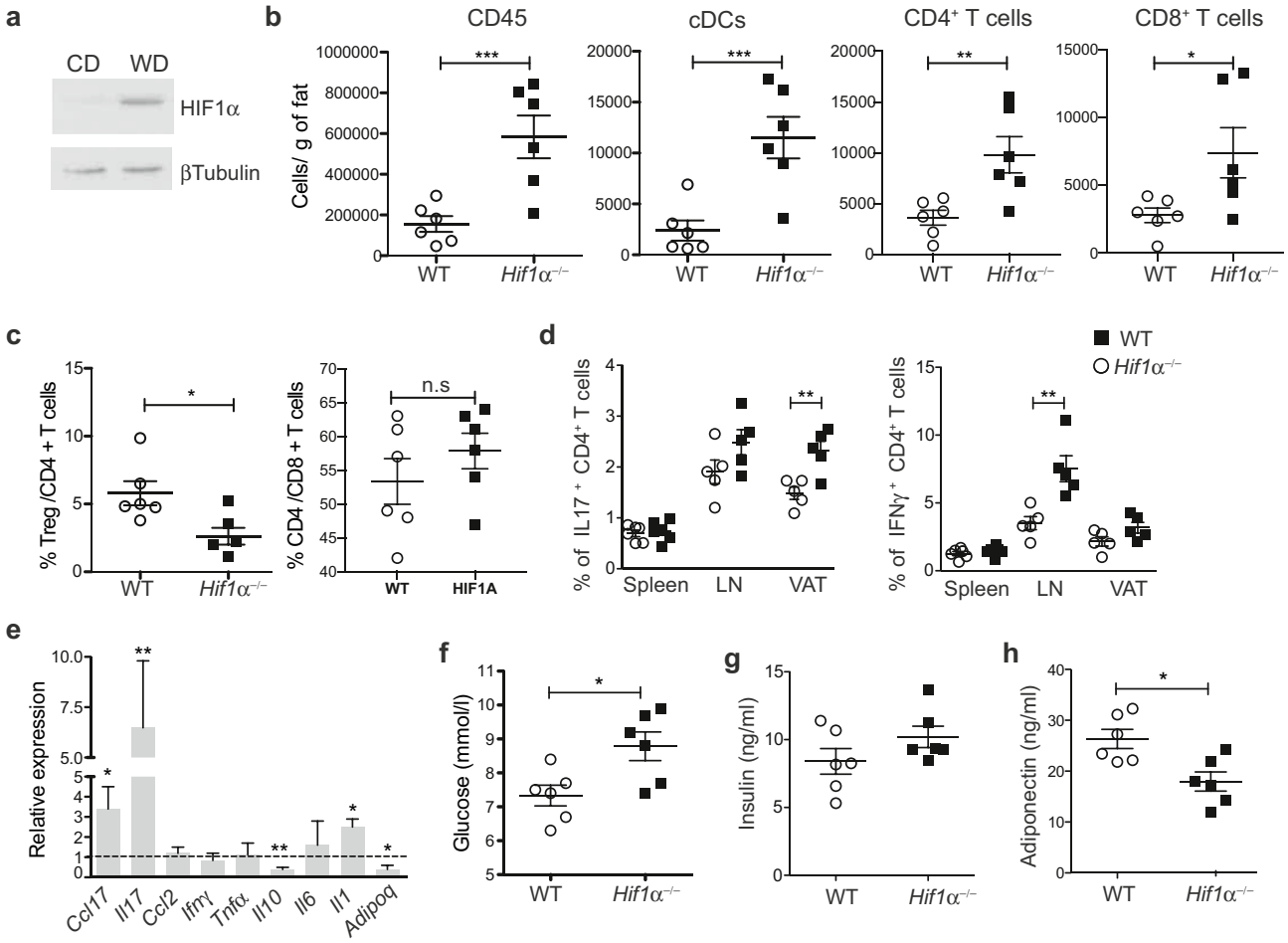

Figure 1. Activation of HIF1α in adipose-tissue cDC ameliorate obesity-induced adipose tissue inflammation. (**a**) Western blot image of HIF1α expression on purified VAT-cDCs. Uncropped image is shown in Suppl. Fig. S4. (**b**) VAT was digested from *Hif1α*$^{-/-}$ and WT mice fed a WD for 12 weeks. Total numbers of CD45$^+$ hematopoietic cells, cDCs, CD4$^+$ and CD8$^+$ T cells were quantified by flow cytometry (n = 6). (**c**) Graph indicate FoxP3$^+$ Tregs/CD4$^+$ and CD4$^+$/CD8$^+$ T cells ratios. (**d**) IL17 and IFNγ production by spleen, LN and VAT-infiltrated CD4$^+$ T cell was evaluated by flow cytometry. Bars represent mean ± SEM (n = 5). (**e**) Quantitative RT-PCR analysis for gene expression in VAT from obese *Hif1α*$^{-/-}$. Expression levels of all genes were normalized against GAPDH RNA and compared to WT mice, which was set as 1. Error bars indicate the geometric mean of 8 biological replicates. (**f**) Fasting glucose, (**g**) insulin and (**h**) adiponectin were detected by ELISA. Bars represent mean ± SEM (n = 6). Statistical analysis was performed with Student's test or one-way ANOVA, $^*p < 0.05$, $^{**}p < 0.01$ and $^{***}p < 0.0005$.

Similarly, HIF1$^{-/-}$ cDCs isolated from VAT an dLN of obese mice showed enhanced OT-II cell proliferation ex vivo compared to WT cDCs (Suppl Fig. S2g). OVA uptake was not affected by *Hif1α* deletion (Suppl Fig. S2h). Thus, depletion of HIF1α in cDCs under sterile conditions appears to unleash their activation.

HIF1α induces intracellular lipid accumulation. Stabilization of HIF1α is known to promote aerobic glycolysis shifting the cells away from glucose oxidative phosphorylation. Upon TLR activation, HIF1α-dependent glycolytic switch enables macrophages and cDCs to produce metabolic intermediates and to fulfil cellular energetic demands required for full activation[22] (Suppl Fig. S3a).

However, HIF1α has recently been shown to regulate mitochondrial glutamine metabolism (Suppl Fig. S3a). Glutamine once converted to α-ketoglutarate (αKG), can be either oxidized to succinate or reduced to isocitrate and then citrate by a mechanism known as reversed TCA cycle. The latter is favoured in cells where HIF1α is stabilized[23,24].

In an attempt to understand the metabolic changes induced by HIF1α in cDCs, we moved to an in vitro system where cDCs were generated from bone-marrow with Flt3 ligand (Flt3L) and Hif1α was activated with desferrioxamine (DFO) (Fig. 3a; Suppl Fig. S3b),which facilitates HIF1 activation during seahorse assays. As expected, DFO induced a glycolytic switch characterized by reduced mitochondria O_2 consumption (OCR) and increased extracellular acidification (ECAR) detected with the XF Mito Stress and the Glycolysis stress test respectively (Fig. 3b). This metabolic shift was HIF1α dependent (Fig. 3b) and equally affecting both main cDC

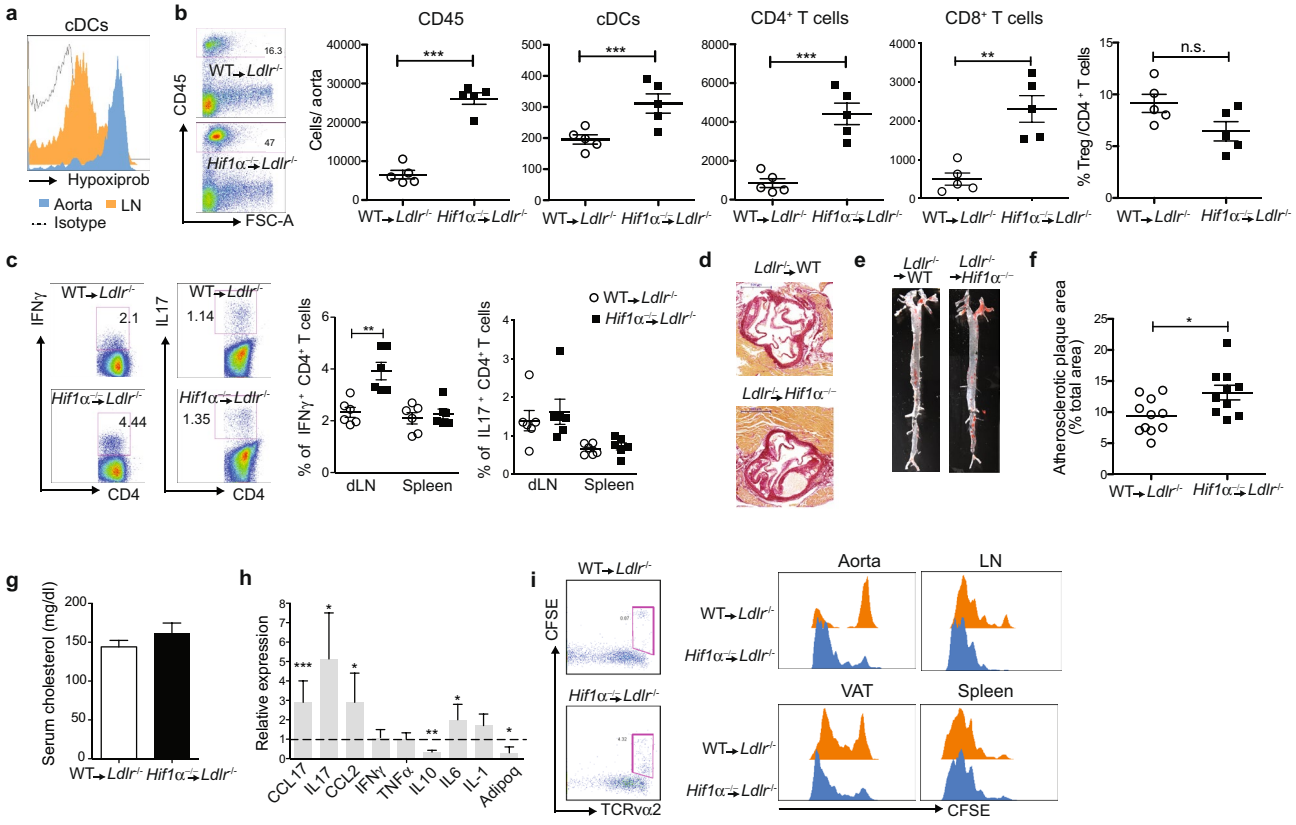

Figure 2. *Hif1α* deletion in cDCs promotes atherosclerotic plaque formation. *Hif1α*$^{-/-}$ → *Ldlr*$^{-/-}$ and WT → *Ldlr*$^{-/-}$ mice were fed a WD for 12 weeks. (**a**) Flow cytometry analysis of aortic-infiltrated cDCs for Hypoxiprobe staining. (**b**) Aorta was enzymatically digested and the presence of CD45^{+} hematopoietic cells, cDCs, CD4^{+} T cells, CD8^{+} T cells and FoxP3^{+} Tregs were quantified by flow cytometry. Representative dot plot from aorta infiltrated CD45^{+} cells. Bars represent mean ± SEM (n = 5). (**c**) IFNγ and IL17 production was analysed by flow cytometry in spleen's and dLN's CD4^{+} T cell. Dot plot is representative of 3 independent experiments. Bars represent mean ± SEM (n = 6). (**d**) Representative Sirius red staining of aortic root. (**e**) Representative images of en face oil red O staining of atherosclerotic lesions in aorta and (**f**) quantification of atherosclerotic lesion size. Bars indicate mean ± SEM (n = 10). (**g**) Total cholesterol in obese mice (n = 10). (**h**) Quantitative RT-PCR analysis for gene expression in perivascular fat from obese *Hif1α*$^{-/-}$. Expression levels of all genes were normalized against GAPDH RNA and compared to WT mice, which was set as 1. Error bars indicate the geometric mean of 7 biological replicates. (**i**) For in vivo antigen presentation, CFSE-labelled OTII cells were transferred i.v. one day before immunization with 200 µg OVA i.p. Three days later, frequency and division of proliferating OT-II T cells were analysed in aorta, LN, VAT and Spleen from Hif1α$^{-/-}$ and WT mice by flow cytometry. Dot plots show gating strategy for CFSE^{+} OTII cells. Histograms show dilution of CFSE^{+} OTII gated cells and are representative of 3 independent experiments. Statistical analysis was performed with Student's test, $^{*}p < 0.05$, $^{**}p < 0.01$ and $^{***}p < 0.0005$.

subsets, cDC1 and cDC2 (Suppl Fig. S3c,d). DFO treatment alone did not affect expression of co-stimulatory molecules (Fig. 3c).

Despite a shift towards aerobic glycolysis, a functional electron transport chain and glutamine-derived carbon may still be required for cellular function. Indeed, in tumour cells, metabolic adaptation under hypoxia involves a switch from glucose to glutamine as a source of carbon for the synthesis of fatty acids[25]. We therefore tested glutamine consumption, which was indeed increased in DFO-treated compared to control cells (Fig. 3d).

During the reverse TCA cycle, glutamine-derived citrate can be transported to the cytoplasm to generate acetyl-CoA, necessary for anabolic reactions such as fatty acid synthesis. In tumour cells, HIF1α-induced uptake and reduction of glutamine induces lipid synthesis and storage in lipid droplets (LD). Interestingly, intracellular accumulation of lipids has been associated with poor cDCs activation and function in tumours[26]. Consistent with an increased glutamine uptake, DFO-treated cells exhibit increased intracellular lipid accumulation in vitro and in vivo as detected by bodipy staining (Fig. 3e,f). Similar results were observed with DMOG and hypoxia treatment (Suppl. Fig. S3e). DFO-induced intracellular lipid accumulation was HIF1α dependent (Fig. 3g). Uptake of C16-Bodipy (palmitate) was unchanged after DFO stimulation in vitro and in vivo suggesting that lipid droplets accumulation is not mediated by lipid uptake but rather lipid synthesis (Fig. 3h,i). Transcriptional levels of the hypoxia-inducible lipid droplet-associated protein (*Hilpda*), which is involved in intracellular neutral lipid deposition, were also elevated after DFO treatment (Fig. 3j).

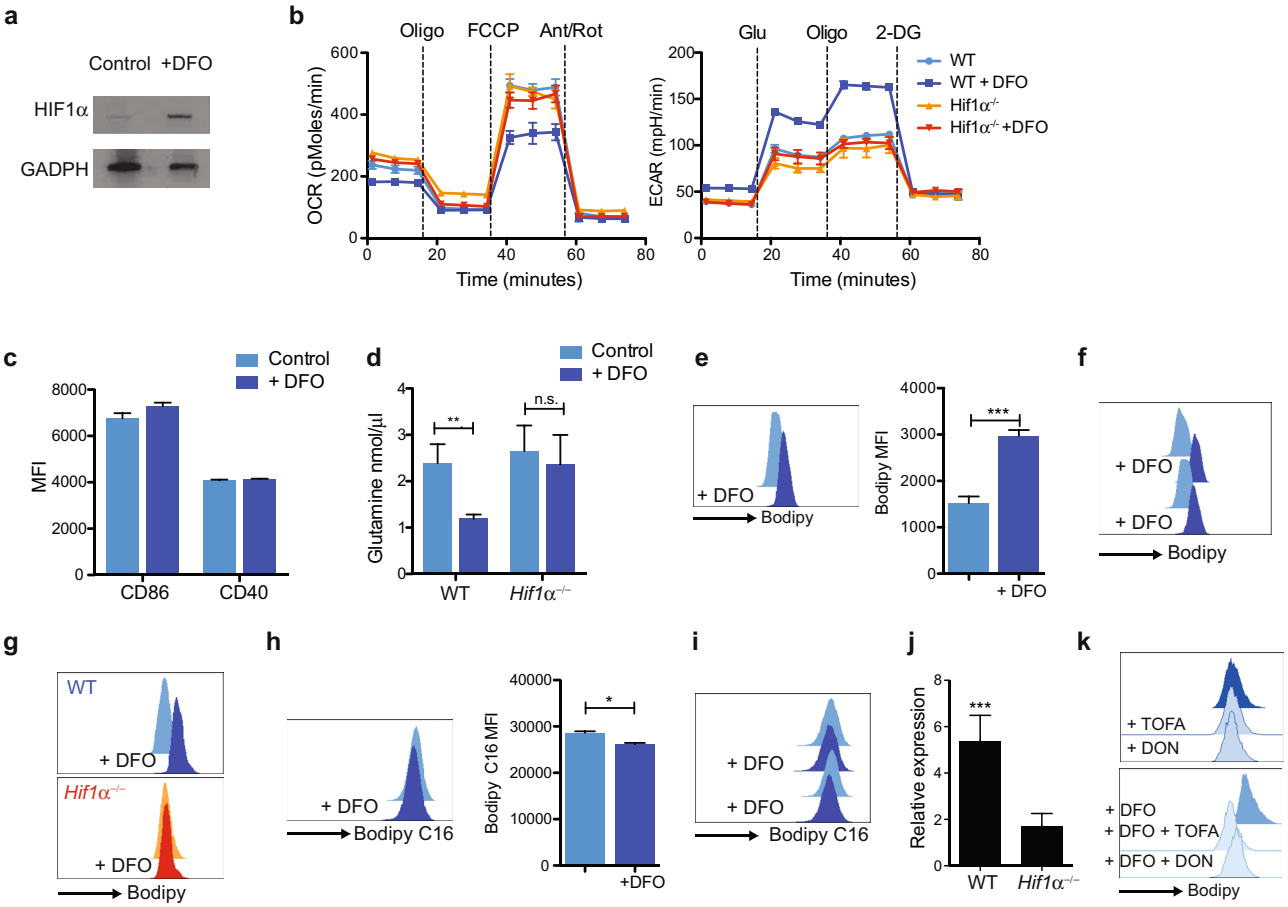

Figure 3. Hif1α activation induces intracellular lipid accumulation. (**a**–**k**) Bone-marrow cells were harvested from WT and Hif1α$^{-/-}$ mice and cultured 7–8 days with recombinant Flt3L to obtain cDCs. Cells were then incubated 1 or 2 days with DFO to activate Hif1α. Uncropped image is shown in Suppl. Fig. S4. (**a**) Expression of Hif1α in cDCs detected by Western blot. (**b**) cDC were purified, counted and plated in a XF96 culture plate. O2 consumption rate (OCR) and medium acidification (ECAR) were measured in real time under basal conditions and in response to indicated inhibitors. Graph are representative of 4 independent experiments. (**c**) Graph indicate expression of CD86 and CD40 in untreated and DFO-treated cells (n-3). (**d**) Glutamine in medium was detected by ELISA (n = 5). (**e**) Intracellular neutral lipids were detected using Bodipy staining by flow cytometry (n = 3). Histogram is representative of 5 independent experiments. (**f**) Bodipy staining from in vivo DFO-treated cDCs. (**g**) Similar to F, but Bodipy stain was performed in control and DFO-treated *Hif1α*$^{-/-}$ and WT cells. Histograms are representative of x independent experiments. (**h**) cDCs were incubated with Bodipy FL C16 to evaluate lipid uptake by flow cytometry (n = 3). (**i**) Bodipy FL C16 staining from in vivo DFO-treated cDCs. (**j**) Quantitative RT-PCR analysis for *Hilpda* expression from WT and *Hif1α*$^{-/-}$ in cDCs upon DFO treatment. Expression level was normalized against GAPDH RNA and compared to untreated conditions, which was set as 1. Error bars indicate the geometric mean of triplicates. (**k**) As in e, but cells were pre-incubated with DFO and then treated with TOFA and DON overnight. Lipid accumulation was detected with Bodipy staining. Histograms are representative of 3 independent experiments. Statistical analysis was performed with Student's test, *p < 0.05, **p < 0.01 and ***p < 0.0005.

To test if glutamine metabolism was responsible for lipid accumulation in cDCs, cells were treated with the fatty-acid synthase inhibitor TOFA and the glutamine antagonist DON. Inhibition of fatty-acid synthesis and glutamine usage, significantly reduced lipid droplets accumulation in DFO-treated cells (Fig. 3k). Collectively, these data suggest that HIF1α activation in cDCs stimulates fatty-acid synthesis and accumulation in lipid droplets.

HIF1α-mediated lipid droplets accumulation suppresses cDC activation. Accumulation of lipids in DCs has been shown to impair their antigen-presenting function in tumours. Mice with deleted expression of HIF1α on cDCs exhibit increased aortic and VAT inflammation. Thus, we tested whether DFO treatment could alter cDCs function in vitro. Indeed, DFO treatment significantly reduces cDCs stimulatory capacity in a mixed-leukocyte reaction (MLR). This effect was reverted after fatty-acid synthesis inhibition with TOFA (Fig. 4a). Similarly, pre-treating cells with DFO reduces cDC cytokine production after LPS treatment (Fig. 4b,c). Thus, similar to tumour-infiltrating DCs, lipid-laden cDC exhibit reduced immunogenicity.

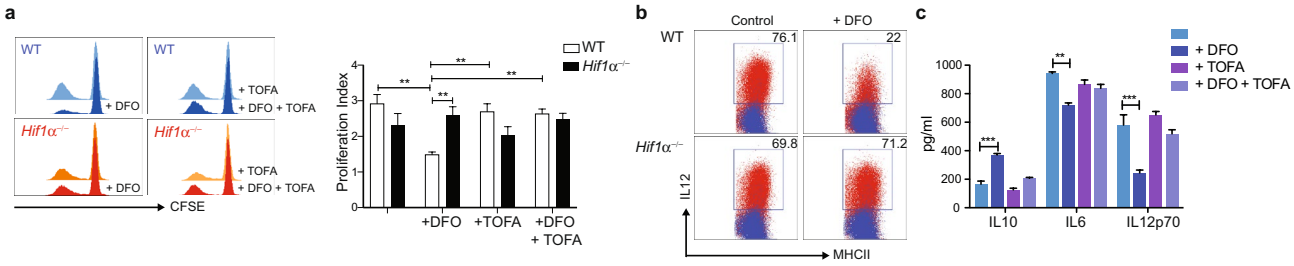

Figure 4. Hif1α activation impairs cDC function. (**a**) Antigen presentation capacity and activation of DFO-treated cDCs was evaluated by MLR. When indicated, cells were also treated with the fatty-acid synthesis inhibitor TOFA. T cell proliferation was assessed by CFSE dilution by flow cytometry. Histograms are representative of 3 independent experiments. Bar graph indicates proliferation index analysed by flow cytometry. (**b**) Cells were treated overnight with DFO and then stimulated with LPS for 6 h or overnight. Intracellular IL-12 production was evaluated by flow cytometry 6 h after stimulation. Dot plots are representative of 3 independent experiments. (**c**) Cytokines were measured in the supernatant WT cDCs after overnight stimulation by ELISA (n = 3). Statistical analysis was performed with one-way ANOVA, $^{**}p < 0.01$ and $^{***}p < 0.0005$.

Lipid accumulation in cDCs alters the expression of lipid mediators. Neutral lipid stored in LD are mobilized by lipases to provide metabolic energy (through fatty acid oxidation) and lipids for membrane synthesis. However, recently, it has become evident that LD function as a major intracellular pool of arachidonic acid, which is the precursor for eicosanoid biosynthesis[27]. In addition, LD can often interact with peroxisomes apparently facilitating peroxisomal fatty acid oxidation[28]. To investigate a possible consequence of lipid accumulation and the synthesis of lipid mediators, we performed a lipid mediator profiling of DFO-treated and control cells (Fig. 5a,b). In these incubations, we identified mediators from all four major fatty acid metabolomes (Table S1). Production of prostaglandins and leukotrienes remained unchanged after DFO treatment, probably due to the absence of TLR stimulation (Table S1). However, incubation of these cells with DFO significantly increased resolvin D2 (RvD2) and thromboxane B_2 (TXB_2) a stable metabolite of TXA_2 (Fig. 5c,d) concentrations. Accordingly, key enzymes contributing to the generation of resolvins were elevated in WT compared to $HIF1^{-/-}$ VAT-cDCs from obese mice (Fig. 5e). RvD2 is a pro-resolving lipid-mediator that was recently shown to suppress T cell responses and to decrease TLR4 expression in monocytes[29]. Similarly, TXA_2 modulates DC-T cell interaction and adaptive immune responses[30]. Interestingly, treatment with RvD2 or deletion of the TXA_2 receptor, TP, significantly delays atherosclerosis progression[31]. Consistent with previous observations, treatment of cDCs-T cell cultures with RvD2 and TP agonist (I-Bop) reduces T cell proliferation in vitro (Fig. 5f). Similarly, the inhibitory effect of HIF1α activation in cDCs, was partially reverted with the TP antagonist SQ29548 (Fig. 5g). Thus, this data suggest that intracellular accumulation of lipids also impacts the production of bioactive lipid mediators by cDC.

Discussion

The transcriptional factor HIF1α plays a central role in cellular adaptation to hypoxia. Physiologic O_2 tension found in tissues varies between 2 and 9%. Hypoxic niches can be observed in a range of tissues including bone marrow, medulla of the kidney, intestinal epithelial and thymus[32–34]. Tissue oxygenation can be severely disrupted during pathological conditions such as obesity, solid tumours, stroke and inflammation leading to hypoxia and HIF1 pathway activation[35–37]. In obesity, HIF1 stabilization is propagated by mitochondrial ROS production[14]. In either of these conditions, HIF1α initiates a transcriptome response to help the cells adapt to a hostile environment. For example, HIF1α induces production of angiogenic factors to promote blood vessel formation; switches cellular metabolism to anaerobic glycolysis; reduces reactive oxygen species (ROS) and upregulates BCL-XL expression thus promoting cell survival[38,39].

The link between HIF1 and inflammation has been increasingly appreciated over recent years. Inflammatory conditions are frequently characterized by tissue hypoxia, ROS production and HIF1α stabilization due to altered metabolic supply/demand ratios[40]. HIF1α activation in adipose tissue hypoxia is a triggering factor for obesity-induced inflammation[41]. Similarly, arterial wall thickening and inflammatory deposition in the atherosclerotic plaque leads to HIF1α stabilization, which appears to promote disease progression[18]. This pro-inflammatory effect appears to be partially mediated by HIF1α activation in myeloid cells. Indeed, mice with myeloid-specific deletion of HIF1α (via lysozyme M-Cre) exhibit improved glucose metabolism, reduced adipose tissue inflammation and decreased atherosclerotic plaque formation[42,43]. With this in mind, we investigated the implications of HIF1α activation in cDCs and its physio-pathological consequences in obesity-induced chronic inflammation.

In this study, we found that inhibition of HIF1α in cDCs promotes adipose tissue inflammation and accelerates the development of atherosclerosis. Deletion of HIF1α appears to unleash cDC activation with an increased in IL12 production and induction of $IL17^+$ T cells. Not apparent difference on lymph node migration and phagocytosis could be detected but this is not an exhaustive study and other mechanisms may be involved. These findings oppose the anti-inflammatory effect observed in myeloid cells. Of note, HIF1 transcription has also been shown to activate multiple anti-inflammatory pathways such as the expression of arginase 1 and VEGF in M2-like tumor-infiltrating macrophages and the upregulation of A2B adenosine receptor promoting Th2 and

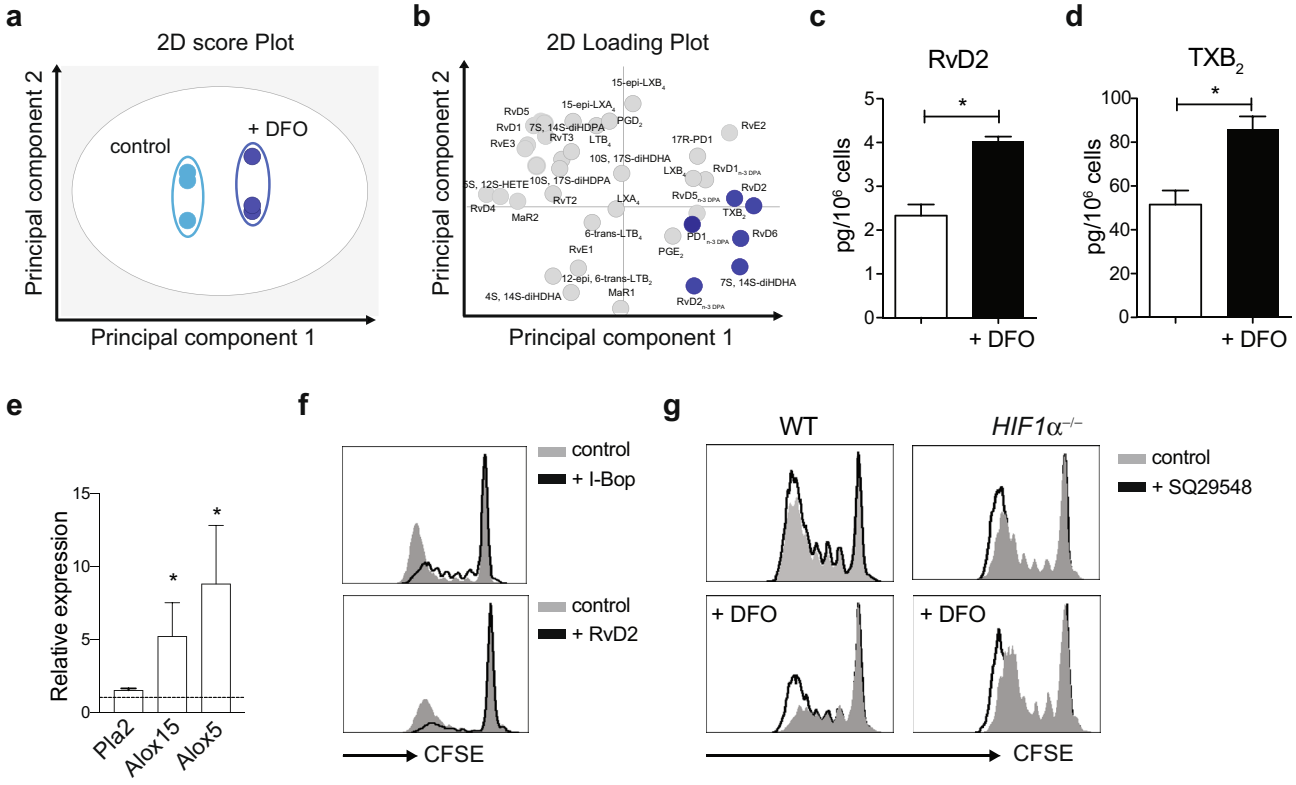

Figure 5. HIF1 stabilization induces changes in the cDC lipid mediator profile. DFO-treated cDCs cells were harvested for lipidomic analysis. Lipid mediators were extracted using solid-phase extraction techniques and identified using liquid chromatography-tandem mass spectrometry-based lipid mediator profiling. (**a**) 2-dimensional score plot of plasma LM-SPM and (**b**) corresponding 2-dimensional loading plot. Gray ellipse in the score plot denotes 95% confidence regions. (**c**) Bars representing significant increase of RvD2, and (**d**) TXB_2 after DFO treatment (n = 3). (**e**) Quantitative RT-PCR analysis for early *Pla2* and late, *Alox15* and *Alox5*, enzymes involved in the synthesis of resolvins in VAT-cDCs from WT and *Hif1α*$^{-/-}$ obese mice. Expression level was normalized against GAPDH RNA and compared to *Hif1α*$^{-/-}$ cDCs, which was set as 1. Error bars indicate the geometric mean of triplicates. WT cDCs were pre-treated with DFO and then the TXA2 agonist I-Bop or RvD2 when indicated. cDC stimulatory capacity was evaluated by MLR. T cell proliferation was assessed by CFSE dilution by flow cytometry. Histograms are representative of 2 independent experiments. (**f**) As in E but T cell were cultured with the TP antagonist SQ29548. Statistical analysis was performed with Student's test, $^{*}p < 0.05$.

Treg differentiation[44]. Therefore, it appears that HIF1 regulates cell effector function in a cell-dependent manner. Contrary to pro-inflammatory macrophages, cDCs in steady-state are poised to suppress immune responses in tissue, which may account for the phenotype observed. Indeed, cDC are important for the control of adipose tissue homeostasis while Flt3L-mediated expansion of cDCs protects mice from atherosclerosis[15,45]. Along those lines, expression of HIF1α in intestinal dendritic cells, which are crucial for the maintenance of mucosal immune homeostasis, suppresses colitis-induced inflammation[12]. These results suggest that activation of HIF1α facilitates cDCs cellular adaptation and survival, allowing them to pursue their anti-inflammatory function.

A key feature of the HIF1 transcriptional response is the upregulation of genes encoding glycolytic enzymes, glucose transporters and the pyruvate dehydrogenase kinase *Pdk1* thereby shunting pyruvate away from mitochondria[6]. Under these conditions, mitochondria are not supplied with glucose-derived acetyl-CoA, a central biosynthetic precursor for lipid synthesis. To compensate for this effect, recent studies in tumor cells have shown a complementary switch towards glutamine metabolism to support anabolism and growth under hypoxic conditions[46]. In cDCs, glutamine-derived lipid synthesis results in the accumulation of lipids in LDs. Interestingly, cDCs in solid tumors, which are in general hypoxic, are also characterized by LD accumulation and an anti-inflammatory phenotype[26]. Indeed, similar findings were described as a result of the ER stress response factor XBP1 activation in ovarian tumor-infiltrated cDCs[47]. XBP1 regulates HIF1α pathway activation and is essential for cell survival under hypoxic conditions[48].

The mechanism by which lipid-laden DCs acquire a tolerogenic function is unclear. Recently it has been suggested that LD in tumor-DCs contain oxidatively truncated electrophilic lipids that interfere with cross-presentation[49]. However, the role of lipid mediators is not known. Lipid mediators are considered key signalling molecules in inflammation as they are locally produced through specific biosynthetic pathways in response to extracellular stimuli[50]. Once produced, they bind to their cognate G protein receptor to exert their function after which they are rapidly inactivated through specific processes[50]. Lipid mediators are involved in many physiological processes and their dysregulation has often been linked to various diseases including atherosclerosis[51]. Lipid mediators

can be subcategorized into different groups, such as AA-derived eicosanoids (e.g. prostaglandins); and the newly identified anti-inflammatory and pro-resolving mediators derived from ω-3 polyunsaturated fatty acids such as resolvins[52]. They can have pro- or anti-inflammatory function: for example, pro-inflammatory lipid mediators, in general terms, include prostaglandins and leukotrienes, while pro-resolving mediators include lipoxins, resolvins, maresins and protectins[52]. The effect of several lipid mediators on DC function is well documented[34,53], however, production of these mediators by cDC and its regulation remains uncharacterized. We here show that activation of HIF1 pathways promotes the expression of RvD2 and TXB_2, two mediators involved in the regulation of T cell responses. The profile of lipid mediators is not only regulated at the enzymatic levels but also through substrate availability that may differ between tissues and physiological and pathological conditions[54]. Our data indicated that HIF1α activation can alter the production of lipid mediators through LD accumulation. How the lipid mediator profile is altered in tissue-cDCs in vivo will require further investigations.

There is currently an increasing interest in targeting immunometabolic pathways in inflammatory diseases and cancer. However, questions arise about the specificity and off-target effect of many metabolic drugs. Although deletion of HIF1α in cDCs results in increased obesity-tissue inflammation, therapeutic treatment with the selective HIF1α inhibitor PX-478 slows down the progression of obesity-induced adipose tissue inflammation[55]. This opposite effect can be mediated through inhibition of HIF1α activation in recruited inflammatory macrophages, inhibition of HIF1-dependent VEGF production or directly on adipocytes[56–59]. Thus, the use of HIF1α inhibitors should be evaluated with caution as it may increase the risk of obesity-induced inflammatory complications such as psoriasis and rheumatoid arthritis or risk of infections.

Methods

Mice. B6.129s7-*Ldlr*^{tm1Her}/J (Ldlr-KO), B6.129-*Hif1a*^{tm3Rsjo}/J (HIFa^{loxp}) and B6.Cg-Tg(TcraTcrb)425Cbn/J (OT-II) mice were purchased from Jackson Laboratory (US); C57BL/6 were purchased from Charles River laboratories (UK); Zbtb46-Cre^{+} mice were kindly provided by Nussenzweig (The Rockefeller University, NY). As previously described[15], mice were housed in temperature- and humidity-controlled rooms at 22 °C and 55% humidity, with a 12 h light/12 h dark cycle. Mice were fed Chow or Test Diet AIN-76A (Test Diet IPS Ltd) and given water ad libitum; animals were rehoused in clean cages weekly. 15 g of Z-NEST (IPS Ltd) was used as nesting material to help regulate temperature and light levels. For chimeras, Ldlr-KO male mice were γ-irradiated twice with 500 rad 3 h apart. Three hours later, mice were reconstituted with marrow cells (3×10^6) that had been harvested from the femurs and tibias of *Hif1α*$^{-/-}$ and control WT littermates. Mice were maintained on acidified water during the critical 4 weeks reconstitution period. Mice fed Western diet that failed to gain more than 20% of body weight were excluded from the study. All animal experimental protocols were carried out in accordance with UK government Home Office licensing procedures and regulations, and approved by QMUL's Animal Welfare and Ethical Review Board (AWERB-7007443).

Flow cytometry staining. VAT was collected from euthanised mice, from the mesenteric, retroperitoneal and abdominipelvic fat depot sites. The tissue was weighed and digested with 2370 U/ml Collagenase II (Sigma) and 23 U/ml DNase (Sigma)/gram of VAT. Immune cells present in the vascular fraction were obtained after centrifugation and lysed of red blood cells before staining. For aortic-single cell preparation, perivascular fat and cardiac muscle was carefully removed and aorta isolated under a dissecting microscope. Aortic segments, including aortic sinus, aortic arch and thoracic aorta were digested with 607.5 U/ml collagenase I, 187.5 U/ml collagenase XI, 90 U/ml hyaluronidase and 90 U/ml DNase in Hank's balanced salt solution for 1 h at 37 °C. Single cell suspensions were stained with fixable Aqua dead cell stain (Invitrogen) to exclude dead cells from analysis and surface markers; DX5-FITC, CD16/32-FITC, F4/80-PerCP, CD206-BV421, CD11c-BV605, CD11c-PE-CY7, CD103-APC, MHCII-AF700, CD11b-AF780, MertK-PE, CD45-PE-CF594, CD64-PE-Cy7, CD8-FITC, Ly6G-BV421, NK1.1-BV605, CD3-AF700, CD3-BV421, CD86-PE, CD4-PE-Cy7, CD4-PeCP-Cy5.5, B220-PerCP, B220-FITC (eBioscience/BioLegend/BD Bioscience/R&D/ThermoFisher). Samples were stained at 4 °C for 30 min and fixed at 4 °C for 30 min with 1% PFA. For intracellular staining of FOXP3-PE (Biolegend), samples were incubated in permeabilization/fixation buffer (eBioscience) at 4 °C for 30 min and washed in permeabilization buffer before staining with fluorescently conjugated primary antibody at 4 °C for 30 min in permeabilization buffer. For hypoxia studies, mice were injected i.p. with 60 mg/kg bw of Hypoxiprobe™-1 (Pimonidazole Hydrochloride, Hypoxiprobe). Two hours later, aortas were harvested, digested and stained with anti-pimonidazole monoclonal antibody-PE (Hypoxiprobe). For intracellular cytokine analysis, immune cells were isolated from tissues and stimulated with 20 ng/ml Phorbol 12-myristate 13-acetate (PMA) (Sigma) and 1 μg/ml Ionomycin (Sigma) for 6 h, in the presence of 10 μg/ml Brefeldin A (Sigma) for the last 5 h. For intracellular staining, samples were first fixed with BD Cytofix/Cytoperm kit (BD Bioscience) and stained for 15 min with IFNγ-APC and IL-17-PE antibodies (Biolegend) following manufacturer's instructions. Samples were then analysed by flow cytometry using a LSR Fortessa (BD Biosciences) and FlowJo version 10 software.

DC innate and adaptive responses. cDC allostimulatory capacity was evaluated in vitro. For this, bone-marrow (BM) cells were harvested from *Hif1α*$^{-/-}$ and WT mice injected previously with B16-Flt3l and cultured in the presence of 0.2 μl/ml recombinant Flt3 ligand (Invitrogen) for 8 days. Cells were then treated with 250 μM DFO (Desferrioxamine, Sigma) overnight. Alternatively, BM-cDCs were treated with DFO for 2 days and 1.2 μM TOFA (5-(Tetradecyloxy)-2-furoic Acid, Sigma) for the last 24 h. CD4^{+} T cells were harvested from the spleen of BALBc mice by CD4^{+} bead positive selection (MACS Miltenyi Biotec) and labelled with CFSE 3 μM (Invitrogen). Cells were mixed at a ratio of 1:5 (5×10^4 CD11c^{+} cDCs: 2.5×10^5 CD4^{+} T cells/well) and incubated for 3–5 days. When applicable, 10 nM of RvD2 (Cayman Chemicals) produced in house, 1 μM of I-BOP ([1S-(1α,2β(5*Z*),3α(1*E*,3*S**),4α)]-7-[3-(3-hydroxy-4-(4′-iodophenoxy)-1-butenyl)-7-oxabicyclo-[2.2.1]

heptan-2-yl]-5-heptenoic acid) or 1 μM of SQ-29548 ([1S-[1α,2α(Z),3α,4α]]-7-[3-[[2-[(phenylamino)carbonyl] hydrazino]methyl]-7-oxabicyclo[2,2,1]hept-2-yl]-5-heptenoic acid,) were added to the cultures. T cell division was assessed by CFSE dilution by flow cytometry and cytokine production in the supernatant by ELISA.

For in vivo cDC T cell stimulatory capacity, mice were injected intravenously with ovalbumin-specific OTII cells purified from spleen and lymph nodes by $CD4^+$ bead positive selection (MACS Miltenyi Biotec) and labelled with CFSE 3 μM (Invitrogen). The next day, mice were immunized with 200 μg of Ovalbumin (Sigma) i.p. Three days later, immune cells were isolated from spleen, lymph nodes, aorta and visceral adipose tissue and OT-II cell division was evaluated by CFSE dilution by flow cytometry. Alternatively, mice were immunized with 200 μg of Ovalbumin (Sigma) i.p. and cDCs from VAT and dLN were isolated four hours later, purified by cell sorting and cultured with CFSE-labelled OT-II cells at a ratio of 1:5 in vitro. CFSE dilution was evaluated by flow cytometry. To evaluate ovalbumin uptake, mice were injected i.p. with 10 μg of OVA-Alexa Fluor-555. Two hours later, visceral adipose tissue was harvested and digested. Ova uptake by cDCs was analysed by flow cytometry.

BM-cDCs were treated with DFO overnight. Cells were then plated at 10^6 cells/well and stimulated with 20 ng/ml LPS (sigma) in the presence of DFO. After culturing overnight, the supernatant was collected and levels of IL-10, IL-6 and IL-12p70 were determined by murine ELISA (eBioscience). Alternatively, cells were stimulated with LPS for 6 h and in combination with 10 μg/ml Brefeldin A (Sigma) for the last 5 h. Intracellular expression of IL-12 was assessed by flow cytometry as previously described. For in vivo IL-12 production, mice were immunized with 1 μg of LPS (Sigma), 2 h later, tissues were harvested, digested and incubated with 10 μg/ml Brefeldin A (Sigma) for an additional 4 h.

Western blotting. Western blotting was performed as describe in[15]. Protein lysates were prepared from purified cDCs using RIPA buffer with phosphatase and protein inhibitors (Pierce). Proteins were separated with SDS-PAGE and transferred to Immobilon™ PVDF membrane (Millipore). Membranes were blocked for 1 h at room temperature in PBST containing 5% (w/v) milk, incubated overnight at 4 °C with anti-Hif1α antibody (Cell signalling) and subsequently with HRP-conjugated secondary antibody (Amersham Bioscience). Blotted proteins were detected using an EZ-ECL™ HRP chemiluminescence detection kit (Biological Industries) and exposed on to Hyperfilm™ photo film (Amersham).

Quantitative Real-time PCR. RT-PCR was performed as previously described[15]. Briefly, RNA from 100 mg VAT was isolated using RNeasy Lipid Tissue Mini Kits (Qaigen) following the manufacturer's instructions. Reverse transcription to cDNA was performed using High-Capacity RNA-to-cDNA Kits (Applied Biosystems) and stored at −80 °C. Gene expression was performed using SYBR Green Supermix (Bio-Rad), according to the manufacturer's instructions, and analysed using a CFX connect light cycler (Bio-Rad). Gene-relative expression was calculated using the ΔΔCT method and normalised to a reference control (GAPDH) with control sample set as 1. Average ratio from replicates was calculated using geometric mean. The following primers were used for the analysis (Invitrogen, UK);

IL10_forward: AAA CAA AGG ACC AGC TGG AC
IL10_reverse: TTC CGA TAA GGC TTG GCA AC
TNFα_forward: TCG TAG CAA ACC ACC AAG TG
TNFα_reverse: TTT GAG ATC CAT GCC GTT GG
IL6_forward: TAG TCC TTC CTA CCC CAA TTT CC
IL6_reverse: TTG GTC CTT AGC CAC TCC TTC
IL1_forward: AAC CTG CTG GTG TGT GAC GTT C
IL1_reverse: CAG CAC GAG GCT TTT TTG TTG T
INFγ_forward: CAG CAA CAG CAA GGC GAA A
INFγ_reverse: CTG GAC CTG TGG GTT GTT GAC
IL17_forward: AAA GCT CAG CGT GTC CAA AC
IL17_reverse: TTC TGG AGC TCA CTT TTG CG
CCL2_forward: GCT GGA GCA TCC ACG TGT T
CCL2_reverse: ATC TTG CTG GTG AAT GAG TAG CA
CCL17_forward: GGA TGC CAT CGT GTT TCT GA
CCL17_reverse: GCC TTC TTC ACA TGT TTG TCT TTG
Alox15_forward: GAC ACT TGG TGG CTG AGG TCTT
Alox15_reverse: TCT CTG AGA TCA GGT CGC TCCT
Alox5_forward: TCT TCC TGG CAC GAC TTT GCT G
Alox5_reverse: GCA GCC ATT CAG GAA CTG GTAG
Pla2g4a_forward: GAT GAG GCT CAA GGA CCC AAA G
Pla2g4a_reverse: GAA TAA AGC CGA GTC GCT CAC C
Apidoq_forward: GAC GTT ACT ACA ACT GAA GAG C
Apidoq_reverse: CAT TCT TTT CCT GAT ACT GGT C
GAPDH_forward: GGC TCA TGA CCA CAG TCC A
GAPDH_reverse: CAC ATT GGG GGT AGG AAC AC

Whole mount aorta and aortic root staining. Immediately after euthanisation, the WD fed mice were flushed free of blood with cold PBS. Using a dissection microscope, the heart and aorta, including the arch with its branching vessels, thorax and abdominal section, were carefully excised and attached fat removed. The aorta was cut away from the heart just above the aortic synapse and both fixed in 4% PFA overnight. The aorta was

opened longitudinally for en face Oil Red O staining. To prepare the stain 3 parts 5 mg/ml Oil Red O solution in isopropanol was diluted with 2 parts distilled water and allowed to solubilise for 1 h prior to 0.45 μm filtration. The aortas were washed in distilled water then transferred into freshly prepared Oil Red O solution for 15 min at room temperature (RT). They were then washed in 60% isopropanol for 5 min. This was repeated until no more red colour came out into the wash. Then the aortas were transferred into distilled water. Glycerol gelatin (Sigma) was used to mount the aortas onto slides and they were visualised using a M205 FA microscope (Leica). Images of the aortas were analysed blindly using ImageJ to quantify the percentage lesion density. The top half of the hearts were paraffin embedded, sectioned and mounted onto slides ready for Sirius Red staining by the BCI Pathology Core Service. The sectioned were visualised using a Pannoramic 250 High Throughput Scanning Microscope.

Lipid mediator profiling. Lipid profiling was performed by QMUL lipidomic facility as described in[60]. Cell incubations were placed in 2 volumes of ice-cold methanol (Thermo Fisher Scientific) containing internal standards (d_8-5S-hydroxy eicosatetraenoic acid, d_5-RvD2, d_5-LXA_4, d_4-PGE_2, and d_4-leukotriene LTB_4 (all from Cayman Chemical); 500 pg each were added to the sample. LMs were extracted and identified as described previously[60]. Briefly, the samples in methanol were incubated for 45 min at − 20 °C for protein precipitation, and centrifuged at 1900*g* at 4 °C for 10 min. The methanol content of the supernatant was evaporated to less than 1 ml using nitrogen gas stream, and the LMs were extracted with automated Extra-Hera system (Biotage, Uppsala, Sweden) employing solid-phase extraction. The methyl formate eluates were concentrated and injected to liquid chromatography-tandem mass spectrometry (LC–MS/MS) system (LC-20AD HPLC (Shimadzu) and SIL-20AC autoinjector (Shimadzu) paired with QTrap 6500 + (ABSciex, Framingham, MA, USA). LMs were identified and quantified using multiple reaction monitoring the parent (Q1) and daughter (Q3) ions in negative ionization mode. Identification was conducted in accordance with published criteria, matching the retention time with authentic and synthetic standards (from Cayman Chemical, prepared in house, or provided by Charles N. Serhan, Harvard Medical School, Boston, MA, USA) and identifying at least 6 diagnostic ions from the MS/MS spectra PMID: 29363065.

Metabolic assays. Adiponectin, Insulin (Merk Millipore), and total cholesterol (Abcam) were measured in the plasma from fasted mice by ELISA. Glucose metabolism was assessed by Glucose (GTT) and Insulin (ITT) tolerance tests after 6 h fasting as previously described in[15]. For GTT, mice were administered with 1.5 mg D-glucose/g of body weight (Sigma) or 0.5 U insulin/kg of body weight (Actrapid) via intraperitoneal injection for ITT. In both cases, blood glucose measurements were taken from tail bleeds at 15, 30, 60, 90, 120, 180 min after injection using blood glucose meter and test strips (FreeStyle Optium Neo, Abbott). Body weight and food intake was recorded weekly. Weight of total visceral adipose tissue harvested was recorded for cell number calculations and to determine the percentage of body weight.

To test mitochondrial respiration and glycolysis, BM-cDCs were treated with DFO overnight and plated at 2×10^5/well onto Seahorse XF96 cell plates. Mito stress and Glycolysis stress test were performed with the Seahorse XF96 Extracellular Flux Analyzer (Agilent) flowing manufacturer's instructions. Glutamine concentration was evaluated in supernatant from overnight DFO-treated BM-cDCs by ELISA (Abcam). For intracellular lipid detection, BM-cDCs were incubated with Bodipy FL or Bodipy-C16 (Invitrogen) at RT for 15 min in PBS. For ex vivo staining, mice were injected 50 μg/g bw DFO i.p. for two consecutive days Mice were euthanised the following day and spleens were digested with 400 U/ml Collagenase D (Roche). Splenocytes were stained with Bodipy FL or Bodipy-C16 as explained above.

Statistical analysis. Statistical analysis was carried out with Graph Prism 8 (GraphPad Software LLC) and significance was evaluated by Student' two tailed *t* test. For GTT and ITT, statistical significance was evaluated with 2-way ANOVA followed by post-hoc Bonferroni test. Differences within means were significant when *P* values of 0.05 or less. Normality was assessed using the Kolmogorov–Smirnov and Shapiro–Wilk test. Data are represented as mean and standard deviation.

Received: 18 May 2020; Accepted: 11 November 2020
Published online: 30 November 2020

References

1. Banchereau, J. & Steinman, R. M. Dendritic cells and the control of immunity. *Nature* **392**, 245–252 (1998).
2. Semenza, G. L. *et al.* Structural and functional analysis of hypoxia-inducible factor 1. *Kidney Int.* **51**, 553–555. https://doi.org/10.1038/ki.1997.77 (1997).
3. Spirig, R. *et al.* Effects of TLR agonists on the hypoxia-regulated transcription factor HIF-1α and dendritic cell maturation under normoxic conditions. *PLoS ONE* **5**, e10983. https://doi.org/10.1371/journal.pone.0010983 (2010).
4. Blouin, C. C., Pagé, E. L., Soucy, G. M. & Richard, D. E. Hypoxic gene activation by lipopolysaccharide in macrophages: Implication of hypoxia-inducible factor 1α. *Blood* **103**, 1124–1130. https://doi.org/10.1182/blood-2003-07-2427 (2004).
5. Tannahill, G. M. *et al.* Succinate is an inflammatory signal that induces IL-1β through HIF-1α. *Nature* **496**, 238. https://doi.org/10.1038/nature11986. https://www.nature.com/articles/nature11986#supplementary-information (2013).
6. Cramer, T. *et al.* HIF-1α is essential for myeloid cell-mediated inflammation. *Cell* **112**, 645–657. https://doi.org/10.1016/S0092-8674(03)00154-5 (2003).
7. Jantsch, J. *et al.* Hypoxia and hypoxia-inducible factor-1α modulate lipopolysaccharide-induced dendritic cell activation and function. *J. Immunol.* **180**, 4697–4705. https://doi.org/10.4049/jimmunol.180.7.4697 (2008).

8. Pantel, A. *et al.* Direct type I IFN but not MDA5/TLR3 activation of dendritic cells is required for maturation and metabolic shift to glycolysis after poly IC stimulation. *PLoS Biol.* **12**, e1001759. https://doi.org/10.1371/journal.pbio.1001759 (2014).
9. Naldini, A. *et al.* Hypoxia affects dendritic cell survival: role of the hypoxia-inducible factor-1α and lipopolysaccharide. *J. Cell. Physiol.* **227**, 587–595. https://doi.org/10.1002/jcp.22761 (2012).
10. Mancino, A. *et al.* Divergent effects of hypoxia on dendritic cell functions. *Blood* **112**, 3723–3734. https://doi.org/10.1182/blood-2008-02-142091 (2008).
11. Yang, M. *et al.* Increased expression of surface CD44 in hypoxia-DCs skews helper T cells toward a Th2 polarization. *Sci. Rep.* **5**, 13674. https://doi.org/10.1038/srep13674 (2015).
12. Fluck, K., Breves, G., Fandrey, J. & Winning, S. Hypoxia-inducible factor 1 in dendritic cells is crucial for the activation of protective regulatory T cells in murine colitis. *Mucosal Immunol.* **9**, 379–390. https://doi.org/10.1038/mi.2015.67 (2016).
13. Lee, Y. S. *et al.* Increased adipocyte O(2) consumption triggers HIF-1α causing inflammation and insulin resistance in obesity. *Cell* **157**, 1339–1352. https://doi.org/10.1016/j.cell.2014.05.012 (2014).
14. Engin, A. Adipose tissue hypoxia in obesity and its impact on preadipocytes and macrophages: hypoxia hypothesis. *Adv. Exp. Med. Biol.* **960**, 305–326. https://doi.org/10.1007/978-3-319-48382-5_13 (2017).
15. Macdougall, C. E. *et al.* Visceral adipose tissue immune homeostasis is regulated by the crosstalk between adipocytes and dendritic cell subsets. *Cell Metab.* **27**, 588-601.e584. https://doi.org/10.1016/j.cmet.2018.02.007 (2018).
16. Makki, K., Froguel, P. & Wolowczuk, I. Adipose tissue in obesity-related inflammation and insulin resistance: cells, cytokines, and chemokines. *ISRN Inflammation* **2013**, 12. https://doi.org/10.1155/2013/139239 (2013).
17. Ross, R. Atherosclerosis–an inflammatory disease. *N. Engl. J. Med.* **340**, 115–126. https://doi.org/10.1056/NEJM199901143400207 (1999).
18. Nakano, D. *et al.* Chronic hypoxia accelerates the progression of atherosclerosis in apolipoprotein E-knockout mice. *Hypertens. Res.* **28**, 837–845. https://doi.org/10.1291/hypres.28.837 (2005).
19. Vink, A. *et al.* HIF-1 a expression is associated with an atheromatous inflammatory plaque phenotype and upregulated in activated macrophages. *Atherosclerosis* **195**, e69–e75. https://doi.org/10.1016/j.atherosclerosis.2007.05.026 (2007).
20. Britton, K. A. & Fox, C. S. Perivascular adipose tissue and vascular disease. *Clin. Lipidol.* **6**, 79–91. https://doi.org/10.2217/clp.10.89 (2011).
21. Ma, Y. *et al.* Hyperlipidemia and atherosclerotic lesion development in Ldlr-deficient mice on a long-term high-fat diet. *PLoS ONE* **7**, e35835. https://doi.org/10.1371/journal.pone.0035835 (2012).
22. Corcoran, S. E. & O'Neill, L. A. J. HIF1α and metabolic reprogramming in inflammation. *J. Clin. Investig.* **126**, 3699–3707. https://doi.org/10.1172/JCI84431 (2016).
23. Sun, R. C. & Denko, N. C. Hypoxic regulation of glutamine metabolism through HIF1 and SIAH2 supports lipid synthesis that is necessary for tumor growth. *Cell Metab.* **19**, 285–292. https://doi.org/10.1016/j.cmet.2013.11.022 (2014).
24. Metallo, C. M. *et al.* Reductive glutamine metabolism by IDH1 mediates lipogenesis under hypoxia. *Nature* **481**, 380–384. https://doi.org/10.1038/nature10602 (2011).
25. Raimundo, N., Baysal, B. E. & Shadel, G. S. Revisiting the TCA cycle: signaling to tumor formation. *Trends Mol. Med.* **17**, 641–649. https://doi.org/10.1016/j.molmed.2011.06.001 (2011).
26. Herber, D. L. *et al.* Lipid accumulation and dendritic cell dysfunction in cancer. *Nat. Med.* **16**, 880. https://doi.org/10.1038/nm.2172 https://www.nature.com/articles/nm.2172#supplementary-information (2010).
27. Guo, Y., Cordes, K. R., Farese, R. V. & Walther, T. C. Lipid droplets at a glance. *J. Cell Sci.* **122**, 749 (2009).
28. Schrader, M., Kamoshita, M. & Islinger, M. Organelle interplay—peroxisome interactions in health and disease. *J. Inherit. Metab. Dis.* https://doi.org/10.1002/jimd.12083 (2019).
29. Chiurchiù, V. *et al.* Proresolving lipid mediators resolvin D1, resolvin D2, and maresin 1 are critical in modulating T cell responses. *Sci. Transl. Med.* **8**, 353ra111 (2016).
30. Kabashima, K. *et al.* Thromboxane A2 modulates interaction of dendritic cells and T cells and regulates acquired immunity. *Nat. Immunol.* **4**, 694. https://doi.org/10.1038/ni943 https://www.nature.com/articles/ni943#supplementary-information (2003).
31. Viola, J. R. *et al.* Resolving lipid mediators Maresin 1 and resolvin D2 prevent atheroprogression in mice. *Circ. Res.* **119**, 1030 (2016).
32. Takubo, K. *et al.* Regulation of the HIF-1α level is essential for hematopoietic stem cells. *Cell Stem Cell* **7**, 391–402. https://doi.org/10.1016/j.stem.2010.06.020 (2010).
33. Hale, L. P., Braun, R. D., Gwinn, W. M., Greer, P. K. & Dewhirst, M. W. Hypoxia in the thymus: role of oxygen tension in thymocyte survival. *Am. J. Physiol. Heart Circ. Physiol.* **282**, H1467–H1477. https://doi.org/10.1152/ajpheart.00682.2001 (2002).
34. Zheng, L., Kelly, C. J. & Colgan, S. P. Physiologic hypoxia and oxygen homeostasis in the healthy intestine. A review in the theme: cellular responses to hypoxia. *Am. J. Physiol. Cell Physiol.* **309**, C350–C360. https://doi.org/10.1152/ajpcell.00191.2015 (2015).
35. Vaupel, P., Kallinowski, F. & Okunieff, P. Blood flow, oxygen and nutrient supply, and metabolic microenvironment of human tumors: a review. *Cancer Res.* **49**, 6449 (1989).
36. Ye, J. Emerging role of adipose tissue hypoxia in obesity and insulin resistance. *Int. J. Obes.* **2005**(33), 54–66. https://doi.org/10.1038/ijo.2008.229 (2009).
37. Ferdinand, P. & Roffe, C. Hypoxia after stroke: a review of experimental and clinical evidence. *Exp. Transl. Stroke Med.* **8**, 9. https://doi.org/10.1186/s13231-016-0023-0 (2016).
38. Chen, N. *et al.* BCL-xL is a target gene regulated by hypoxia-inducible factor-1α. *J. Biol. Chem.* **284**, 10004–10012. https://doi.org/10.1074/jbc.M805997200 (2009).
39. Robey, I. F., Lien, A. D., Welsh, S. J., Baggett, B. K. & Gillies, R. J. Hypoxia-inducible factor-1α and the glycolytic phenotype in tumors. *Neoplasia (New York, N.Y.)* **7**, 324–330 (2005).
40. Eltzschig, H. K. & Carmeliet, P. Hypoxia and Inflammation. *N. Engl. J. Med.* **364**, 656–665. https://doi.org/10.1056/NEJMra0910283 (2011).
41. Halberg, N. *et al.* Hypoxia-inducible factor 1α induces fibrosis and insulin resistance in white adipose tissue. *Mol. Cell. Biol.* **29**, 4467–4483. https://doi.org/10.1128/mcb.00192-09 (2009).
42. Takikawa, A. *et al.* HIF-1α in myeloid cells promotes adipose tissue remodeling toward insulin resistance. *Diabetes* **65**, 3649 (2016).
43. Aarup, A. *et al.* Hypoxia-inducible factor-1α expression in macrophages promotes development of atherosclerosis. *Arterioscler. Thromb. Vasc. Biol.* **36**, 1782 (2016).
44. Colegio, O. R. *et al.* Functional polarization of tumour-associated macrophages by tumour-derived lactic acid. *Nature* **513**, 559. https://doi.org/10.1038/nature13490 (2014).
45. Choi, J. H. *et al.* Flt3 signaling-dependent dendritic cells protect against atherosclerosis. *Immunity* **35**, 819–831. https://doi.org/10.1016/j.immuni.2011.09.014 (2011).
46. Gameiro, P. A. *et al.* In vivo HIF-mediated reductive carboxylation is regulated by citrate levels and sensitizes VHL-deficient cells to glutamine deprivation. *Cell Metab.* **17**, 372–385. https://doi.org/10.1016/j.cmet.2013.02.002 (2013).
47. Cubillos-Ruiz, J. R. *et al.* ER stress sensor XBP1 controls anti-tumor immunity by disrupting dendritic cell homeostasis. *Cell* **161**, 1527–1538. https://doi.org/10.1016/j.cell.2015.05.025 (2015).
48. Chen, X. *et al.* XBP1 promotes triple negative breast cancer by controlling the HIF1 α pathway. *Nature* **508**, 103–107. https://doi.org/10.1038/nature13119 (2014).

49. Veglia, F. *et al.* Lipid bodies containing oxidatively truncated lipids block antigen cross-presentation by dendritic cells in cancer. *Nat. Commun.* **8**, 2122. https://doi.org/10.1038/s41467-017-02186-9 (2017).
50. Shimizu, T. Lipid mediators in health and disease: enzymes and receptors as therapeutic targets for the regulation of immunity and inflammation. *Annu. Rev. Pharmacol. Toxicol.* **49**, 123–150. https://doi.org/10.1146/annurev.pharmtox.011008.145616 (2009).
51. Fredman, G. *et al.* An imbalance between specialized pro-resolving lipid mediators and pro-inflammatory leukotrienes promotes instability of atherosclerotic plaques. *Nat. Commun.* **7**, 12859. https://doi.org/10.1038/ncomms12859 https://www.nature.com/articles/ncomms12859#supplementary-information (2016).
52. Serhan, C. N., Chiang, N., Dalli, J. & Levy, B. D. Lipid mediators in the resolution of inflammation. *Cold Spring Harb. Perspect. Biol.* **7**, a016311. https://doi.org/10.1101/cshperspect.a016311 (2015).
53. Shi, Q. *et al.* PGE2 elevates IL-23 production in human dendritic cells via a cAMP dependent pathway. *Mediat. Inflamm.* **2015**, 984690. https://doi.org/10.1155/2015/984690 (2015).
54. Schlager, S. *et al.* Adipose triglyceride lipase acts on neutrophil lipid droplets to regulate substrate availability for lipid mediator synthesis. *J. Leukoc. Biol.* **98**, 837–850. https://doi.org/10.1189/jlb.3A0515-206R (2015).
55. Sun, K., Halberg, N., Khan, M., Magalang, U. J. & Scherer, P. E. Selective inhibition of hypoxia-inducible factor 1α ameliorates adipose tissue dysfunction. *Mol. Cell. Biol.* **33**, 904–917 (2013).
56. Maier, A. *et al.* Hypoxia-inducible protein 2 Hig2/Hilpda mediates neutral lipid accumulation in macrophages and contributes to atherosclerosis in apolipoprotein E-deficient mice. *FASEB J.* **31**, 4971–4984. https://doi.org/10.1096/fj.201700235R (2017).
57. Akhtar, S. *et al.* Endothelial hypoxia-inducible factor-1α promotes atherosclerosis and monocyte recruitment by upregulating microRNA-19a. *Hypertension* **66**, 1220–1226 (2015).
58. Jiang, C. *et al.* Disruption of hypoxia-inducible factor 1 in adipocytes improves insulin sensitivity and decreases adiposity in high-fat diet-fed mice. *Diabetes* **60**, 2484–2495. https://doi.org/10.2337/db11-0174 (2011).
59. Kihira, Y. *et al.* Deletion of hypoxia-inducible factor-1α in adipocytes enhances glucagon-like peptide-1 secretion and reduces adipose tissue inflammation. *PLoS ONE* **9**, e93856. https://doi.org/10.1371/journal.pone.0093856 (2014).
60. Dalli, J., Colas, R. A., Walker, M. E. & Serhan, C. N. Lipid mediator metabolomics via LC–MS/MS profiling and analysis. *Methods Mol. Biol. (Clifton, N.J.)* **1730**, 59–72. https://doi.org/10.1007/978-1-4939-7592-1_4 (2018).

Acknowledgements

We are grateful to M. Nussenzweig (The Rockefeller University) for providing the Zbtb46-Cre mice. We thank George Elia at QMUL for all histology assistance. This work was supported by the British Heart Foundation FS/14/66/31293 (C.E.M.), FS/13/49/30421 (M.P.L., H.B.), PG/16/79/32419 (M.P.L., E.G.W.), Barts Charity (MGU0441) and Marie Curie/Cascade CF-2013-11-003-longhi (M.P.L.).

Author contributions

M.P.L. conceive the study; E.G.W., F.M.B. and M.P.L. designed experiments; E.G.W., C.E.M., H.B., and M.P.L. performed and analysed experiments. M.C. provided technical support for atherosclerosis model; J.D. and R.A.C. performed lipidomic analysis and synthesis of lipid mediators. E.G.W. and M.P.L. wrote the manuscript.

Competing interests

The authors declare no competing interests.

Additional information

Supplementary information is available for this paper at https://doi.org/10.1038/s41598-020-77793-6.

Correspondence and requests for materials should be addressed to M.P.L.

Reprints and permissions information is available at www.nature.com/reprints.

Publisher's note Springer Nature remains neutral with regard to jurisdictional claims in published maps and institutional affiliations.